Journal of Electroanalytical Chemistry 895 (2021) 115363

Contents lists available at ScienceDirect

Journal of Electroanalytical Chemistry

journal homepage: www.elsevier.com/locate/jelechem

Diffusion coefficient and nucleation density studies on electrochemical deposition of aluminum from chloroaluminate ionic liquid electrolytes

Yuxiang Peng, Pravin S. Shinde, Ramana G. Reddy *

Department of Metallurgical and Materials Engineering, The University of Alabama, Tuscaloosa, AL 35487, USA

ARTICLE INFO

Keywords:
Ionic liquid
Aluminum
Cyclic voltammetry
Chronoamperometry
Diffusion coefficient

ABSTRACT

In this study, aluminum was electrodeposited from ionic liquids comprising a melt of alkyl imidazolium chlorides and aluminum chloride ($AlCl_3$). The ionic liquids utilized in this study were 1-ethyl-3-methyl-imidazolium chloride (EMIC)-$AlCl_3$, 1-butyl-3-methylimidazolium chloride (BMIC)-$AlCl_3$, and 1-hexyl-3-methyl-imidazolium chloride (HMIC)-$AlCl_3$ at the $AlCl_3$ mole fraction of 0.667 (molar ratio of 1:2). The electrochemical behavior of chloroaluminate species in the three ionic liquids was investigated by cyclic voltammetry (CV) and chronoamperometry (CA) techniques at different temperatures. The cyclic voltammograms indicated that the reduction of $Al_2Cl_7^-$ species to metallic aluminum followed a diffusion-controlled phenomenon. Moreover, even at a less negative applied potential, the higher current density was obtained for EMIC-$AlCl_3$ ionic liquid. That indicates that EMIC-$AlCl_3$ favors less energy consumption during the electrodeposition. The chronoamperometric analysis revealed that the onset of aluminum deposition from such ionic liquids proceeds via a three-dimensional instantaneous nucleation process. The concentrations of $Al_2Cl_7^-$ ions in the ionic liquids were calculated based on the thermodynamic data, which were 2520, 2271, and 2035 mol m^{-3} for EMIC-$AlCl_3$, BMIC-$AlCl_3$, and HMIC-$AlCl_3$, respectively. The diffusion coefficient (D) values of $Al_2Cl_7^-$ species in such ionic liquids were also calculated at various temperatures. The D values determined from the CA technique at 363 K are 2.16×10^{-11}, 1.03×10^{-11}, and 0.87×10^{-11} $m^2\ s^{-1}$ for EMIC-$AlCl_3$, BMIC-$AlCl_3$, and HMIC-$AlCl_3$, respectively. In addition, the D value increased as temperature increased and decreased as the hydrocarbon group in the ionic liquid increased. The calculated grain sizes of nucleation range from 2 to 4 μm for these ionic liquids and are in good agreement with experimental data obtained from SEM micrographs.

1. Introduction

Aluminum, which makes up about 8% of the earth's crust, is the third most abundant element, following oxygen and silicon [1]. Since no metallic phase exists in nature, nearly all aluminum is produced in the electrolyte form via electrodeposition [2]. The industrial process of aluminum production is the Hall-Heroult process, which is a process of aluminum extraction from a high-temperature cryolite bath. For further purification, the Hoopes process and segregation process are used to refine the aluminum [3]. However, such conventional methods require high temperatures (above 1073 K) that consume lots of energy and release unwanted greenhouse gases [3]. Therefore, the notion of extraction and refining the aluminum from low-temperature ionic liquid (IL) electrolyte is attracting immense interest since the last decade [4]. In addition, the advantage of the electrodeposition method is that the coating of aluminum or its alloy can be achieved to promise high corrosion resistance and electric conductivity [5].

The IL is an eco-friendly and efficient electrolyte due to its non-corrosive property, the wide temperature range for the liquid phase, excellent thermal stability, low vapor pressure, wide electrochemical window, and low pollutant emission [6–8]. Therefore, the ILs have been used as electrolytes to electrodeposit numerous pure metals or alloys, especially those that are hard to be prepared in an aqueous solution [5,9]. A few electrochemical studies of aluminum and its alloy in different ILs have been studied by several researchers [6,10–13]. Several ILs have been used to electrodeposit Al, which are formed by the combination of $AlCl_3$ with alkyl imidazolium chlorides such as 1-ethyl-3-methyl-imidazolium chloride (EMIC)-$AlCl_3$, 1-butyl-3-methylimidazolium chloride (BMIC)-$AlCl_3$, or 1-hexyl-3-methyl-imidazolium chloride (HMIC)-$AlCl_3$. Although $AlCl_3$ is in a solid phase at room temperature, the mixture of $AlCl_3$ with M(= E, B, H)MIC quickly transforms into a liquid phase at room temperature. The mixture of the melt leads to the formation of several chloroaluminate anions, which exits in equilibrium, according to the following reactions (1–3) [14,15].

* Corresponding author at: Department of Metallurgical and Materials Engineering, The University of Alabama, P. O. Box 870202, Tuscaloosa, AL 35487, USA.
E-mail address: rreddy@eng.ua.edu (R.G. Reddy).

https://doi.org/10.1016/j.jelechem.2021.115363
Received 26 January 2021; Received in revised form 6 April 2021; Accepted 10 May 2021
Available online 16 May 2021

$$AlCl_3 + Cl^- \overset{Room\ Temperature}{\Longleftrightarrow} AlCl_4^- \quad (1)$$

$$AlCl_3 + AlCl_4^- \overset{Room\ Temperature}{\Longleftrightarrow} Al_2Cl_7^- \quad (2)$$

$$AlCl_3 + Al_2Cl_7^- \overset{Room\ Temperature}{\Longleftrightarrow} Al_3Cl_{10}^- \quad (3)$$

The amount of $AlCl_3$ determines the Lewis acidity of the MMIC-$AlCl_3$ melt. When the molar ratio of $AlCl_3$ and MMIC is less than 1, the melt consists of organic cation and tetra-chloroaluminate ions ($AlCl_4^-$). In melts containing the excess of $AlCl_3$ (molar ratio > 1), the excess $AlCl_3$ reacts with $AlCl_4^-$ anions to form Lewis acidic hepta-chloroaluminate ions ($Al_2Cl_7^-$) [16].

The electrochemical kinetics of reducing such chloroaluminate anion species to aluminum is necessary to be discussed in such ILs before the electrodeposition or electrorefining. The process of electrolysis of aluminum in $AlCl_3$-BMIC [17] and $AlCl_3$-EMIC [18] ILs has been illustrated previously using the cyclic voltammetry (CV) method. The chronoamperometry (CA) method has been used to describe the nucleation process of aluminum as the instantaneous process in $AlCl_3$-BMIC [6,17] and $AlCl_3$-EMIC [6,18–20] ILs. In addition, based on the CA method, the diffusion coefficient and the number of nucleation density of Al species in those ionic liquids are calculated [6,19,20]. However, little research is performed on the diffusion process of aluminum species in these three ILs systematically, especially for the $AlCl_3$-HMIC IL. Although few literature studies discuss that the electrodeposition process is due to the diffusion of $Al_2Cl_7^-$ species [6,18,21], the effect of temperature, viscosity, and hydrocarbon group on the diffusion process is still unclear. And some of the literature investigated the diffusion coefficient of Al species in such ILs based on the planar diffusion process. However, little literature considers the effect of cylindrical electrode, which will cause little error in the calculation of diffusion coefficient if considering the planar diffusion.

In this study, the melts of $AlCl_3$ with EMIC, BMIC, and HMIC ILs are utilized to study aluminum electrodeposition. The CV and CA experiments are performed to analyze the mechanism of diffusion and deposition of aluminum species from such ILs. The concentration of $Al_2Cl_7^-$ species is calculated based on the densities of ILs and fraction of Al species in the ILs. In addition, the diffusion coefficients of $Al_2Cl_7^-$ species in such ILs are calculated by different methods, including the cylindrical-diffusion method at various temperatures. It was found that the diffusion coefficient increased as temperature increased while it decreased as the hydrocarbon group of the IL increased. Moreover, the IL's larger viscosity will also result in the lower diffusion coefficient of $Al_2Cl_7^-$ species. Besides, aluminum's nucleation process is studied using the CA method, which is a three-dimensional instantaneous nucleation process. Finally, the number density of nucleation and grain sizes of nucleation are determined based on the instantaneous model and compared with the experimental result performed with scanning electron microscopy (SEM).

2. Experimental details

2.1. Materials

The chemicals such as $AlCl_3$ (95%), EMIC (95%, HPLC), BMIC (98%, HPLC), and HMIC (97%, HPLC) single salts were purchased from Sigma-Aldrich. In the present work, the MMIC to $AlCl_3$ molar ratio of 1:2 was used to maximize the concentration of $Al_2Cl_7^-$ anion species in the ILs. Before the mixing process, the MMIC was placed in a vacuum oven to dry for at least 6 h. The chemicals were then weighed in an appropriate ratio in a glove box under dry ultra-high purity (UHP, 99.995%) argon (Ar) gas. The MMIC was taken in a 250 mL beaker, and then $AlCl_3$ was slowly added into it at room temperature. A glass rod was used to stir while adding the $AlCl_3$. When the IL becomes a clear solution, it is transferred to another 50 mL beaker, placed on a hot plate, and stirred for about 30 min for homogeneous mixing using a magnetic stirrer at 60 rpm. The temperature of the pre-heated hot plate was set to the experimental temperature (353 K).

2.2. Methods

The electrochemical experiments were performed with an EG&G PARC model 273 A potentiostat/galvanostat instrument controlled by Power Suite software. Several CV curves were obtained by varying the scan rate from 100 to 300 mV s^{-1}. The CA curves were obtained by changing the overpotentials. The CV and CA experiments were performed from MMIC-$AlCl_3$ ILs using a three-electrode cell configuration. And each CV and CA experiment was repeated at least two times to ensure repeatability. Fig. 1 shows the schematic of the experimental setup.

As shown in Fig. 1, the temperature was controlled by a hot plate and was precisely monitored by the inserted thermometer. Tungsten (W) wire (99.9%) with a diameter of 0.45 mm was used as a working electrode, aluminum wire with 1-mm diameter was used as a counter electrode, and the reference electrode was Pt wire (99.9%) with a 0.5 mm diameter. The W was used as a working electrode because it is stable in Lewis acidic ionic liquid electrolytes and doesn't undergo any chemical or electrochemical reactions in the studied experimental potential regime. The W has been employed as a working electrode in previous studies involving ionic liquid electrolytes [6]. The Ar gas flow was continuously maintained through the alumina tube during the experiment. Thus, the whole system was under the argon gas atmosphere. All the electrodes were ground with 800 grit SiC abrasive paper, washed with acetone and deionized water, and dried by air right before the experiment. The height of the electrode immersed into the IL was measured after the experiment for area normalization.

3. Results and discussion

3.1. Concentration of $Al_2Cl_7^-$ in ionic liquid

Before the CV or CA experiments, densities of ILs were calculated and extrapolated based on the literature data [22] to calculate the volume and the concentration of the total Al species in the electrolyte, which is listed in Table 1. Based on the distribution of Al species in IL using the thermodynamic calculations [22,23], the mole fraction of $Al_2Cl_7^-$ anions is 0.7831 for the 1:2 molar ratio of MMIC to $AlCl_3$. The mole fraction of other anions like $Al_3Cl_{10}^-$ and $AlCl_4^-$ are about 0.1 in the ionic liquid. In addition, this thermodynamic distribution of Al species in EMIC-$AlCl_3$ has been proved with the Raman experiment [24]. And the fractions between $AlCl_4^-$ and $Al_2Cl_7^-$ species are in good agreement between thermodynamic and experimental results. Whatever the species $AlCl_3$ transfers, it will combine with one MMIC to form the complex ion. Thus, the total amount of Al species ($AlCl_4^-$, $Al_2Cl_7^-$ or $Al_3Cl_{10}^-$) is equal to the amount of MMIC species. Therefore, the concentration of $Al_2Cl_7^-$ anions is calculated using the following relation (4).

$$C_{Al_2Cl_7^-} = C_{MMIC} * 0.7831 \quad (4)$$

where $C_{Al_2Cl_7^-}$ is the concentration of $Al_2Cl_7^-$ (mol m^{-3}),C_{MMIC} is the concentration of the MMIC species (mol m^{-3}), and 0.7831 is the fraction of $Al_2Cl_7^-$ anion among all the anion species. Based on the known densities, the concentration of $Al_2Cl_7^-$ anions in different ILs is also calculated, as shown in Table 1.

3.2. Cyclic voltammetry method

3.2.1. Cyclic voltammetry curves

For electrochemical studies, use of Al as a reference electrode is reported in the literature as it is stable in ionic liquid electrolytes

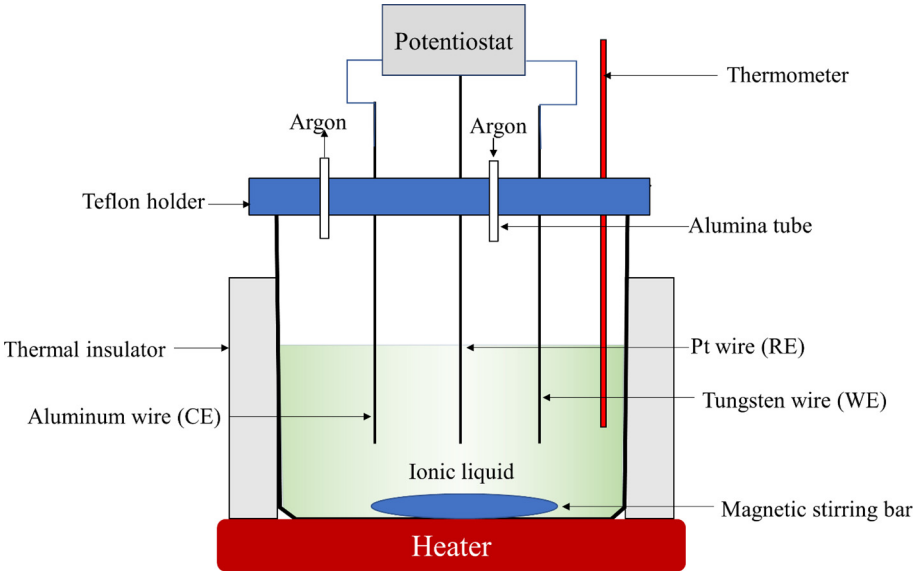

Fig. 1. Schematic of an electrochemical cell for CV and CA experiments in ILs.

Table 1
Densities and concentration of $Al_2Cl_7^-$ in each IL with 1:2 molar ratio.

Temperature (K)	EMIC-$AlCl_3$ Density (kg m^{-3})	Concentration of $Al_2Cl_7^-$ (mol m^{-3})	BMIC-$AlCl_3$ Density (kg m^{-3})	Concentration of $Al_2Cl_7^-$ (mol m^{-3})	HMIC-$AlCl_3$ Density (kg m^{-3})	Concentration of $Al_2Cl_7^-$ (mol m^{-3})
353	1340	2539	1290	2289	1230	2052
363	1330	2520	1280	2271	1220	2035
373	1320	2501	1270	2253	1210	2019
383	1310	2482	1260	2236	1210	2019

[6,25]. However, in our present study, the CV curves were performed from three ionic liquid electrolytes with Pt as reference electrode. Because, Pt is also stable in the ionic liquid electrolytes, and no chemical reaction happens between Pt and Al ions. Sweeping the applied potential or the temperature variance does not affect the stability of the Pt reference electrode. The suitability of Pt as a reference electrode has been investigated and it is a proper reference electrode in the aqueous electrochemical experiments [26]. Additionally, Pt has also been used as the reference for non-aqueous electrolyte such as EMIC-$AlCl_3$ ionic liquid to study the electrodeposition of Al [21]. Before the experiments, a CV was performed to investigate the potential windows of these ionic liquids. The potential window regimes of the pristine EMIC, BMIC and HMIC ionic liquid electrolytes are shown in the Fig. 2. The potential windows of these ionic liquids are slightly different but the magnitude of potential window is in the range of 2.6–2.8 V for a given reference electrode. The reduction potential starts at −1.78 V, −2.0 V, and −1.95 V vs. Pt for EMIC, BMIC and HMIC, respectively.

To investigate the electrochemical behavior of aluminum species in MMIC-$AlCl_3$ electrolyte, the CVs were performed on a tungsten wire electrode from three IL electrolytes at different scan rates (100–300 mV s^{-1}) at 363 K, as shown in Fig. 3. The measured area of the tungsten wire working electrode immersed in the IL was 2.5×10^{-5} m^2 for EMIC-$AlCl_3$, 2.7×10^{-5} m^2 for BMIC-$AlCl_3$, and 2.3×10^{-5} m^2 for HMIC-$AlCl_3$. The reference electrode is Pt.

As shown in Fig. 3, the reduction peak potential of Al deposition is slightly higher than the negative potential window. However, the initial electrodeposition potential of Al is in the range of the stable potential window of the pristine ionic liquid (without $AlCl_3$). The CV curves reveal the cathodic peak currents (A) with potential at approximately −1.9 V for EMIC-$AlCl_3$, −2.3 V for BMIC-$AlCl_3$, and −2.7 V for

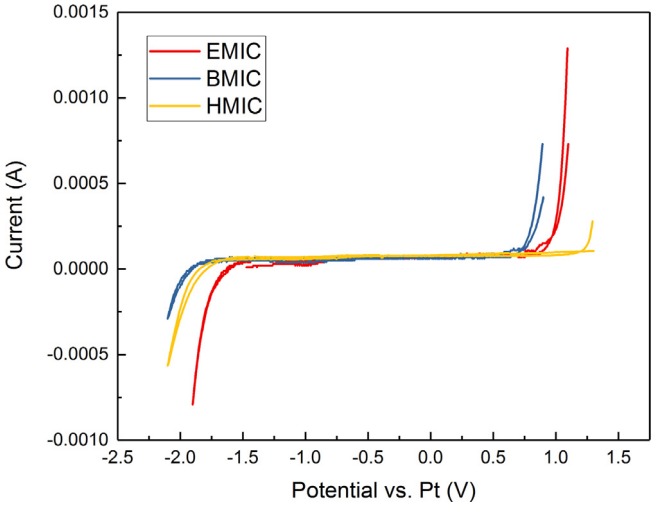

Fig. 2. Cyclic voltammetry curves recorded on W-electrode at 100 mV/s vs. Pt RE from EMIC, BMIC and HMIC electrolytes solvents (without $AlCl_3$).

HMIC-$AlCl_3$ IL. In addition, the corresponding anodic peak current (A') is also noticeable during the reverse sweep. According to the literature [6,12,15], the cathodic peak and anodic peak are attributed to the formation and dissolution of aluminum, respectively. The corresponding reactions are shown below (Equations (5) & (6)).

$$\text{Cathode}: 4Al_2Cl_7^- + 3e^- \rightarrow \text{Al} + 7\text{AlCl}_4^- \quad (5)$$

$$\text{Anode}: \text{Al} + 7\text{AlCl}_4^- \rightarrow 4Al_2Cl_7^- + 3e^- \quad (6)$$

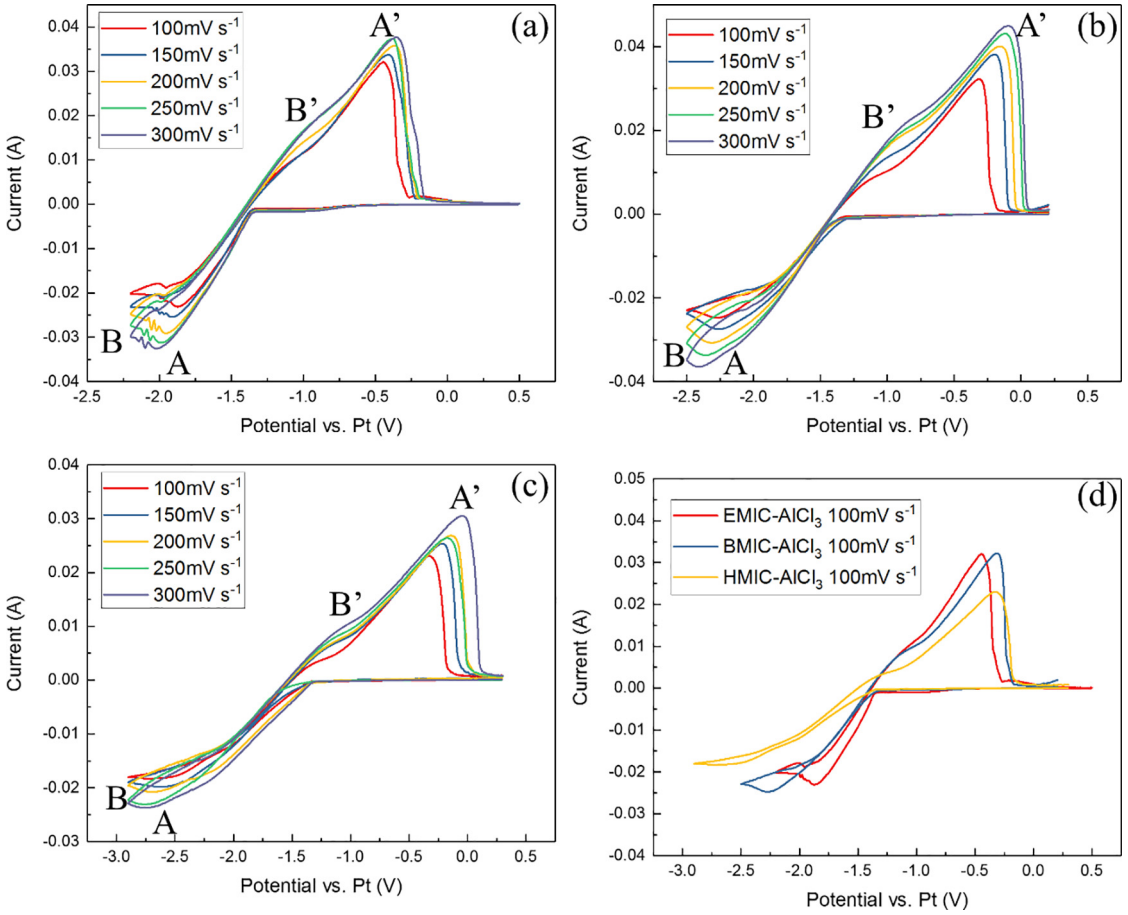

Fig. 3. CV curves of (a) EMIC-$AlCl_3$, (b) BMIC-$AlCl_3$, (c) HMIC-$AlCl_3$ (molar ratio: 1:2) using tungsten working electrode and aluminum counter electrode at 363 K, and (d) comparison of CV curves for three ILs. Area of working electrode is 2.5×10^{-5} m^2 for EMIC-$AlCl_3$, 2.7×10^{-5} m^2 for BMIC-$AlCl_3$, and 2.3×10^{-5} m^2 for HMIC-$AlCl_3$.

The $Al_2Cl_7^-$ anions present in the IL are diffused to the cathode and get discharged in the form of Al deposition. The $AlCl_4^-$ anions then react with the formed Al deposits to produce $Al_2Cl_7^-$ ions. According to the reaction listed in equations (5 & 6), the number of transferred electrons is 0.75 mole for 1 mole $Al_2Cl_7^-$ anion diffusion.

Besides, another anodic current peak (B') is observed before the current peak (A'), which causes the reverse sweep to shift at different scan rates. And the corresponding cathodic peak current is assumed to be at around point (B). As the 3-electron oxidation of deposited Al to Al^{3+} is a one-step reaction the evidence of two oxidation peaks signifies the stripping of Al to produce different Al anion species (mainly, $Al_3Cl_{10}^-$ and $Al_2Cl_7^-$). The redox reactions corresponding to B and B' might be related to the discharging and recharging of $Al_3Cl_{10}^-$ species. Since there is little concentration of $Al_3Cl_{10}^-$ anion species in the IL electrolyte according to the distribution of Al species [22], the possible reactions are shown by equations (7) and (8) below [27].

$$\text{Cathode}: 2Al_3Cl_{10}^- + 3e^- \rightarrow \text{Al} + 5AlCl_4^- \quad (7)$$

$$\text{Anode}: \text{Al} + 5AlCl_4^- \rightarrow 2Al_3Cl_{10}^- + 3e^- \quad (8)$$

The exact reactions and mechanisms at points B and B' are still unclear and more evidence is needed to confirm them. However, the reduction reaction (point B) due to the trace amount of $Al_3Cl_{10}^-$ species is ignored in the investigation of Al deposition's kinetics. As shown in Fig. 3, the current densities of reduction and oxidation peaks (A and A') increase with increasing scan rate in these IL electrolytes. As shown in Fig. 3(d) and Table 2, the cathode peak current density in HMIC-$AlCl_3$ ionic liquid presents the lowest value at the same scanning rate. In addition, the potentials corresponding to the peak currents become more negative as the hydrocarbon group increased. To study the mechanism of the diffusion process of $Al_2Cl_7^-$ anion species, several parameters obtained from CV curves are recorded. Table 2 lists the parameters obtained from the CV curve of EMIC-$AlCl_3$, BMIC-$AlCl_3$, and HMIC-$AlCl_3$ at 363 K.

3.2.2. Diffusion coefficient calculated with the Randles-Sevcik equation

For the diffusion-controlled quasi-reversible process, the diffusion coefficient of $Al_2Cl_7^-$ ions in MMIC-$AlCl_3$ IL can be calculated by the Randles-Sevcik (R&S) equation (9) [28].

$$I_{pc} = 0.4958nFAC_i\left(\frac{\alpha nF}{RT}\right)^{0.5} D^{0.5}\nu^{0.5} \quad (9)$$

where I_{pc} is the cathodic peak current (A), A is the area of working electrode (m^2), R is the gas constant (8.314 J K^{-1} mol^{-1}), T is the experimental temperature (K), n is the number of exchanged electrons (0.75), and F is the Faraday constant (96485C mol^{-1}). C_i is the bulk concentration of $Al_2Cl_7^-$ ions (mol m^{-3}), D is the diffusion coefficient (m^2 s^{-1}), ν is the potential scan rate (V s^{-1}), and α is the charge transfer coefficient.

For the quasi-reversible electron transfer process, the value of the charge transfer coefficient can be determined by the Nicholson and Shain equation (10) [28].

$$\left|E_{pc} - E_{pc/2}\right| = 1.857RT/\alpha nF \quad (10)$$

where E_{pc} is the cathodic peak potential (V), $E_{pc/2}$ is the cathodic half-peak potential (V), which is determined by the potential corresponding to the half-peak current.

Table 2
The values of cathodic peak potential (E_{pc}), anodic peak potential (E_{pa}), the separation between the cathodic peak potential, and cathodic half-peak potential ($|E_{pc}-E_{pc/2}|$), and cathodic peak current density (j_{pc}) for EMIC-$AlCl_3$, BMIC-$AlCl_3$ and HMIC-$AlCl_3$ under different scan rates at 363 K.[#]

Scan rate (mV s^{-1})	E_{pc} (mV)	E_{pa} (mV)	$\|E_{pc}-E_{pa}\|$ (mV)	$\|E_{pc}-E_{pc/2}\|$ (mV)	$\|j_{pc}\|$ (A m^{-2})
EMIC-$AlCl_3$					
100	−1874	−444	−1429	324	924
150	−1911	−410	−1501	337	1016
200	−1953	−365	−1588	374	1160
250	−1990	−381	−1609	395	1248
300	−2019	−354	−1665	411	1300
BMIC-$AlCl_3$					
100	−2267	−313	−1954	548	916
150	−2276	−199	−2077	592	1016
200	−2311	−157	−2154	586	1137
250	−2355	−119	−2236	616	1248
300	−2411	−96	−2316	648	1348
HMIC-$AlCl_3$					
100	−2596	−329	−2267	736	796
150	−2623	−219	−2404	723	861
200	−2695	−143	−2552	858	900
250	−2736	−175	−2561	786	1004
300	−2755	−46	−2709	886	1030

[#] Note: The area of tungsten working electrode immersed in the IL is 2.5 × 10^{-5} m^2 for EMIC-$AlCl_3$, 2.7 × 10^{-5} m^2 for BMIC-$AlCl_3$, and 2.3 × 10^{-5} m^2 for HMIC-$AlCl_3$. The reference electrode is Pt.

The transfer coefficient is calculated to be around 0.21, 0.13 and 0.10 in EMIC-$AlCl_3$, BMIC-$AlCl_3$ and HMIC-$AlCl_3$, respectively, which are different from the reported transfer coefficients: 0.4 in BMIC-$AlCl_3$ (1.5) [22] and 0.45 in TMPAC-$AlCl_3$ (2.0) [29]. The CV experiments were not under mass transportation controlled sufficiently by a rotating electrode. In addition, the mass transfer may contribute much to those highly viscous ionic liquids. Therefore, the calculated transfer coefficients are not the very exact value. However, all the calculated transfer coefficients, including the reported data, are less than 0.5, indicating that the forward and reverse electron transfer steps are not symmetric in the cyclic voltammetry. And transfer coefficient will affect the activation energy of the reaction from oxidation to reduction. For a reversible process, the E_p should be independent of the scan rate. However, in the present study, the E_p has shifted, meaning that the process is not reversible. For a reversible process, E_{pa}-E_{pc} = 57/n mV (n is the number of transferred electrons). For our case, it varied from 476 to 555 mV for EMIC-$AlCl_3$, 651 to 771 mV for BMIC-$AlCl_3$, and 755 to 903 mV for HMIC-$AlCl_3$. In addition, the passivation behavior of Al in the ionic liquid has been proved [4], which also may affect the reversible process during the CV experiment.

As different scan rates were applied in the experiments, one can plot the graph of j_{pc} vs. $\nu^{0.5}$. With the known slope, the R&S equation (9) can be modified and written as equation (11).

$$slope\ of\ \left(j_{pc}\ vs.\nu^{0.5}\right) = 0.4958nFC_i\left(\frac{\alpha nF}{RT}\right)^{0.5} D^{0.5} \quad (11)$$

where j_{pc} is the current density (A m^{-2}). And the plot of j_{pc} vs. $\nu^{0.5}$, as shown in Fig. 4.

As shown in Fig. 4, the plot of j_{pc} vs. $\nu^{0.5}$ does not pass through the origin point. The intercepts indicate the plot is not perfectly fitted with the R&S equation. One reason might be a kinetic current contributes to the cathodic peak current [18]. The other reason is due to the cylindrical electrode used in the experiment, but the R&S equation is derived based on planar diffusion.

3.3. Diffusion coefficient and nucleation density using chronoamperometry method

3.3.1. Diffusion coefficient of $Al_2Cl_7^-$

The CA experiments are performed to evaluate the mechanism of Al deposition in the ILs, including nucleation and growth mechanism. The chronoamperometric current–time transients for three different

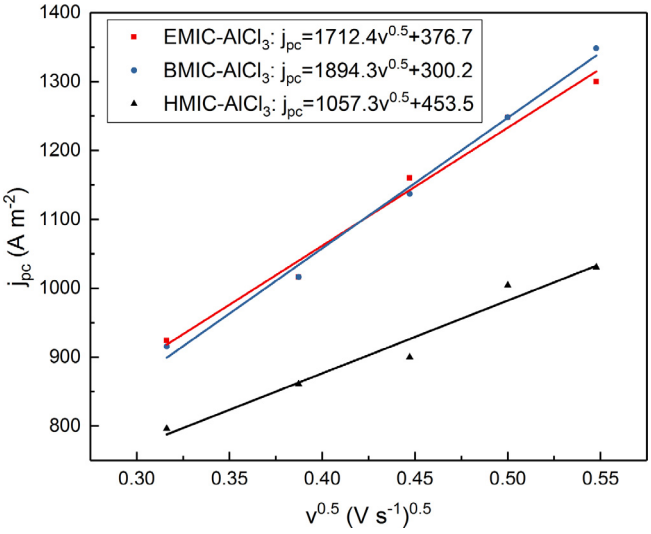

Fig. 4. The cathodic peak current density (j_{pc}) obtained in Table 1 as a function of the square root of scan rate ($\nu^{1/2}$) in E(B, H)MIC-$AlCl_3$ IL at 363 K.

ILs at different applied potentials at 363 K are shown in Fig. 5. The tungsten working electrode area immersed in the IL is 2.90 × 10^{-5} m^2 for EMIC-$AlCl_3$, 2.43 × 10^{-5} m^2 for BMIC-$AlCl_3$, and 3.96 × 10^{-5} m^2 for HMIC-$AlCl_3$, respectively. The reference electrode was Pt.

As shown in Fig. 5, the applied overpotentials are sufficient to initiate the nucleation and growth of aluminum as the maximum current (I_m) and corresponding time (t_m) were observed. A similar phenomenon was also found in the lead [30], zinc [31], and aluminum as reported by other researchers [4,6,18]. In Fig. 5 (b), the current increased initially at a specific maximum value and then dropped. However, in Fig. 5(a) and (c), the current initially declined due to the double layer charging between the tungsten electrodes and then increased to the current peak [6]. After time t_m, the current decreased with time slowly. One explanation illustrates that it is due to the diffusion-limited steady-state process, where aluminum nuclei formed hemispherical diffusion zones. When the zones overlap, the linear mass-transfer process is dominated [32,33]. Another explanation is that the overlapped nucleation reduced the activity of the atom

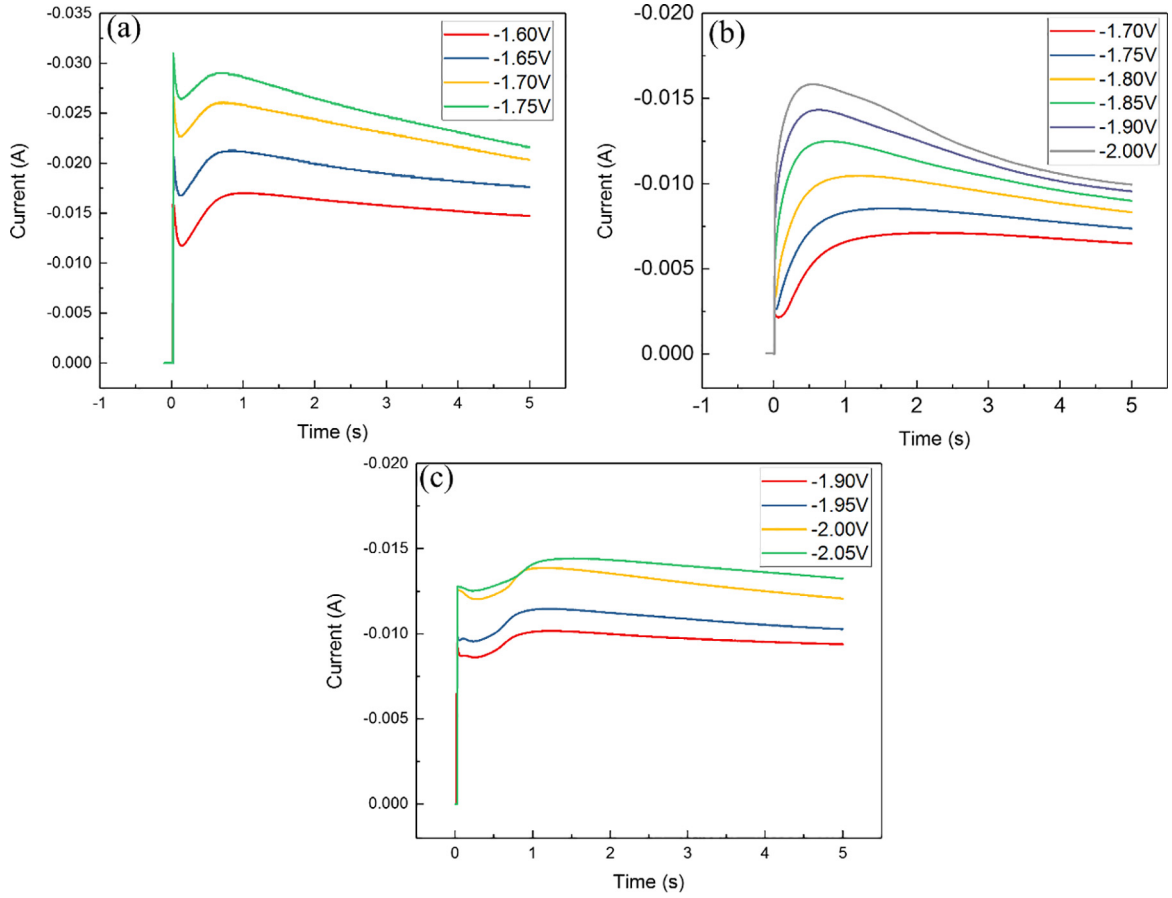

Fig. 5. The chronoamperometric current–time transients for Al deposition in (a) EMIC–$AlCl_3$, (b) BMIC–$AlCl_3$, and (c) HMIC–$AlCl_3$ ILs with different overpotentials at 363 K (Area of working electrode = 2.90×10^{-5} m^2 for EMIC-$AlCl_3$, 2.43×10^{-5} m^2 for BMIC-$AlCl_3$, and 3.96×10^{-5} m^2 for HMIC-$AlCl_3$).

incorporation to the crystal lattice [30]. Moreover, when the applied overpotential is more negative, the value of the maximum current is increased while the corresponding time is decreased. As the cathodic potential increased, the nucleation rate and density of aluminum are increased [34].

The nucleation process of aluminum adatoms on the foreign substrate is related to some kind of three-dimensional nucleation process. The dimensionless experimental current–time transients is compared with the dimensionless theoretically instantaneous and progressive nucleation model, which is described by Scharifker and Hills [32]. The detailed expression is listed in equations (12–13), which present the relationship between dimensionless current density (j/j_m) to the dimensionless time (t/t_m).

$$Instantaneous: \ (j_{inst}/j_m)^2 = 1.9542(t_{inst}/t_m)^{-1}\{1-\exp[-1.2564(t_{inst}/t_m)]\}^2 \quad (12)$$

$$Progressive: \ (j_{prog}/j_m)^2 = 1.2254(t_{prog}/t_m)^{-1}\left\{1-\exp\left[-2.3367(t_{prog}/t_m)^2\right]\right\}^2 \quad (13)$$

where j is the current density (A cm^{-2}) at any experimental time t, j_m is the maximum current density, and t_m time (s) is its corresponding time. The correction of the delay time, t_o, is calculated according to the estimated linear plot of $(I/I_m)^2$ vs. time [35]. And the estimated value of t_o is much lower than that of t_m. Thus, the correction value is ignored during this comparison and t_o has an insignificant influence on the experimental plot. The dimensionless current–time transients for different potentials in three ILs at 363 K along with theoretical nucleation processes are compared, as shown in Fig. 6.

As shown in Fig. 6, the experimental results are closely relatable to the instantaneous nucleation process, especially when the time is before t_m. However, for the longer time, the experimental currents are larger than the theoretical values from the instantaneous nucleation model, reportedly due to partial kinetic control of the growth process or some minor reactions [30,34]. The sharp rise and drop of current is usually ascribed to a transition from spherical diffusion into a slower planar diffusion, as the diffusion radii from multiple growing particles eventually overlap. Although it is not convincing to say but based on our study, the model fits well and do not interfere because the curve before the current maximum t_m matches with the instantaneous nucleation model. In addition, the nucleation processes at other temperatures also follow the instantaneous nucleation process. A similar nucleation process is reported by several other researchers [4,6,18].

Since the Al electrodeposition follows the three-dimensions nucleation and diffusion process, the diffusion coefficient of $Al_2Cl_7^-$ anion can be estimated by considering the instantaneous model illustrated by Scharifker and Hills (S&H) [32], according to equation (14).

$$j_m^2 t_m = 0.1629(nFC_0^*)^2 D \quad (14)$$

where the values of j_m and t_m are obtained in Fig. 5, n is transferred electrons (0.75 mole for 1 mole $Al_2Cl_7^-$ diffusion), F is Faraday constant (96485C mol^{-1}), C_0 is the concentration of $Al_2Cl_7^-$ and D is diffusion coefficient (m^2 s^{-1}). The diffusion coefficients of $Al_2Cl_7^-$ anion in three ILs at different temperatures are calculated using the S&H method by taking the average value at different potentials. The calculated diffusion coefficients at 363 K are 8.94, 4.61, and 4.44×10^{-11} m^2 s^{-1} in EMIC-$AlCl_3$, BMIC-$AlCl_3$, and HMIC-$AlCl_3$, respectively.

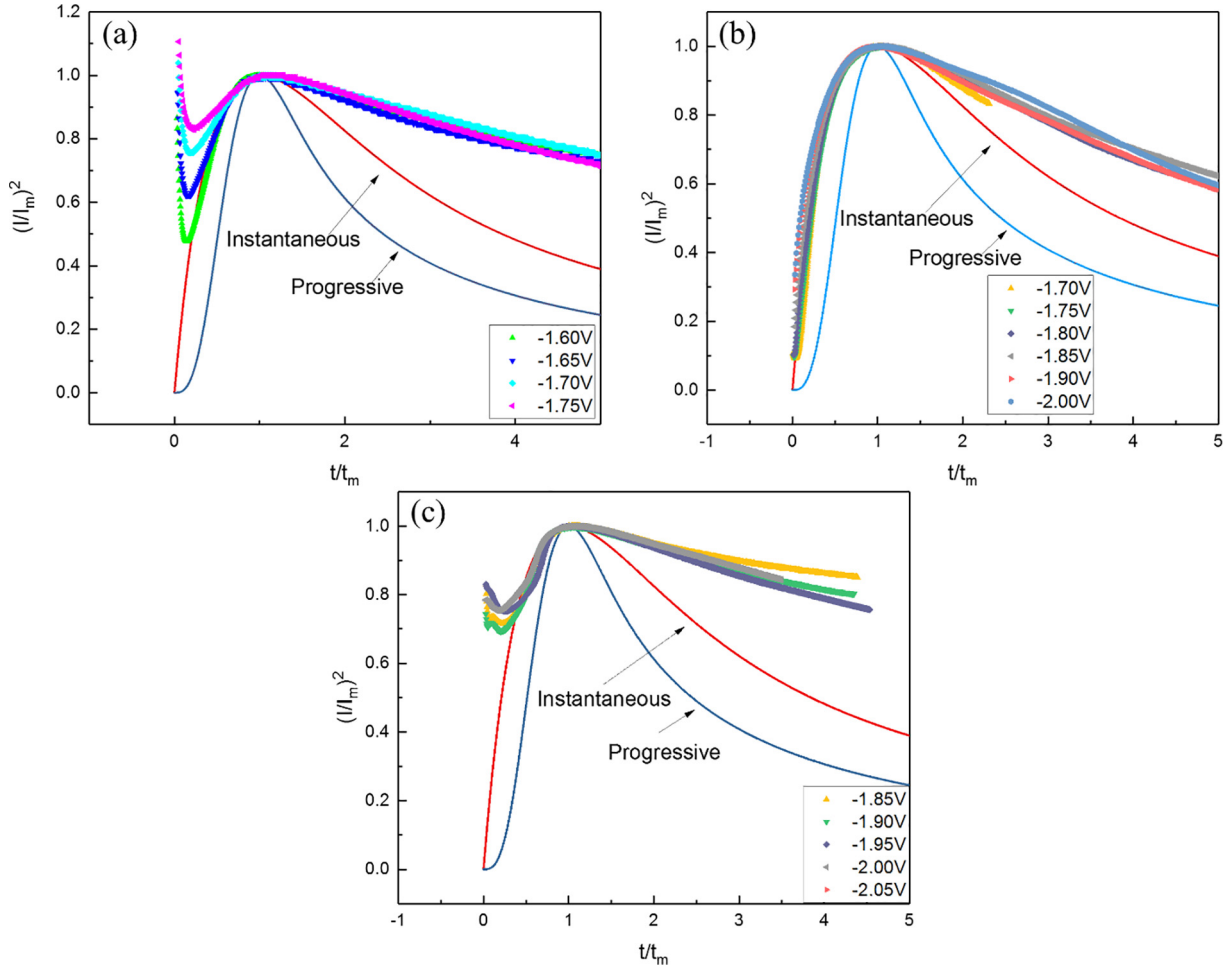

Fig. 6. Comparison between experimental current–time transients at different potentials, different ILs ((a) EMIC-$AlCl_3$, (b) BMIC-$AlCl_3$, and (c) HMIC-$AlCl_3$) and theoretical instantaneous and progressive nucleation at 363 K.

As discussed earlier, during CV experiments, the electrodeposition of Al is a diffusion-controlled process; then the Cottrell equation can also be applied to estimate the diffusion coefficient of $Al_2Cl_7^-$ using equation (15) [28].

$$I = nFAD^{0.5}C_0(\pi t)^{-0.5} \tag{15}$$

where I is current (A), A is an area of the working electrode (m^2), n, F, C_0, D have been mentioned in equation (14), and t is the time (s).

Although this method cannot be directly applied in the electrodeposition process, estimating the diffusion coefficient of $Al_2Cl_7^-$ is still available [6]. In addition, at 363 K, the current obtained in the decreasing portion (Fig. 5) follows a linear relationship with the reciprocal square root of time ($t^{-0.5}$), as shown in Fig. 7. The Cottrell plot is more like a linear relationship at a longer-time domain (lower value of $t^{-0.5}$). Therefore, more accurate slopes obtained at a longer-time domain are considered in the calculation of the diffusion coefficient of $Al_2Cl_7^-$ anion species. The average value is regarded as the final calculated result of the diffusion coefficient. And the results at 363 K are 3.71, 2.37, and 0.38 $\times$ 10^{-11} m^2 s^{-1} in EMIC-$AlCl_3$, BMIC-$AlCl_3$, and HMIC-$AlCl_3$, respectively.

However, equations (14 & 15) are derived based on the planar diffusion, but experiments were performed with a cylindrical electrode (tungsten wire). In addition, because of the partial kinetic control of the growth process or some minor reactions at a longer-time domain, the experimental data does not fit the theoretical instantaneous nucleation model well. The value calculated by the Cottrell method (equation (15)) in this portion may not be very accurate. The intercepts shown in Fig. 6abc also indicate that the relationship between current and $t^{-0.5}$ does not follow Cottrell's equation well because the linear relationship does not pass through the origin.

Therefore, there is another revised method to calculate the diffusion coefficient based on the cylindrical electrode. For the cylindrical electrode, the chronoamperometry experiment's current and time is more likely follows the equation (16) [36].

$$I = \frac{nFADC_0}{a\ln\left(1+\sqrt{\pi Dt}/a\right)} \tag{16}$$

where I, A, n, F, C_0, D, and t have been mentioned in equation (14 & 15), and a is the radius of the working electrode, which is 2.25 $\times$ 10^{-4} m.

However, it is complicated to obtain the D value directly from equation (16). The numerical solution was obtained using MATLAB at every point of current versus time under each applied potential. As the process at the initial time (before t_m) fits very well with the theoretical instantaneous nucleation process, the average diffusion coefficient was calculated by considering the data point at that portion. Thus, the mean value of the diffusion coefficients calculated at different applied potentials was taken as the final value for a given temperature. The results are shown in Fig. 8.

As shown in Fig. 8, the diffusion coefficient of $Al_2Cl_7^-$ increased as temperature increased. In addition, the diffusion coefficient of $Al_2Cl_7^-$

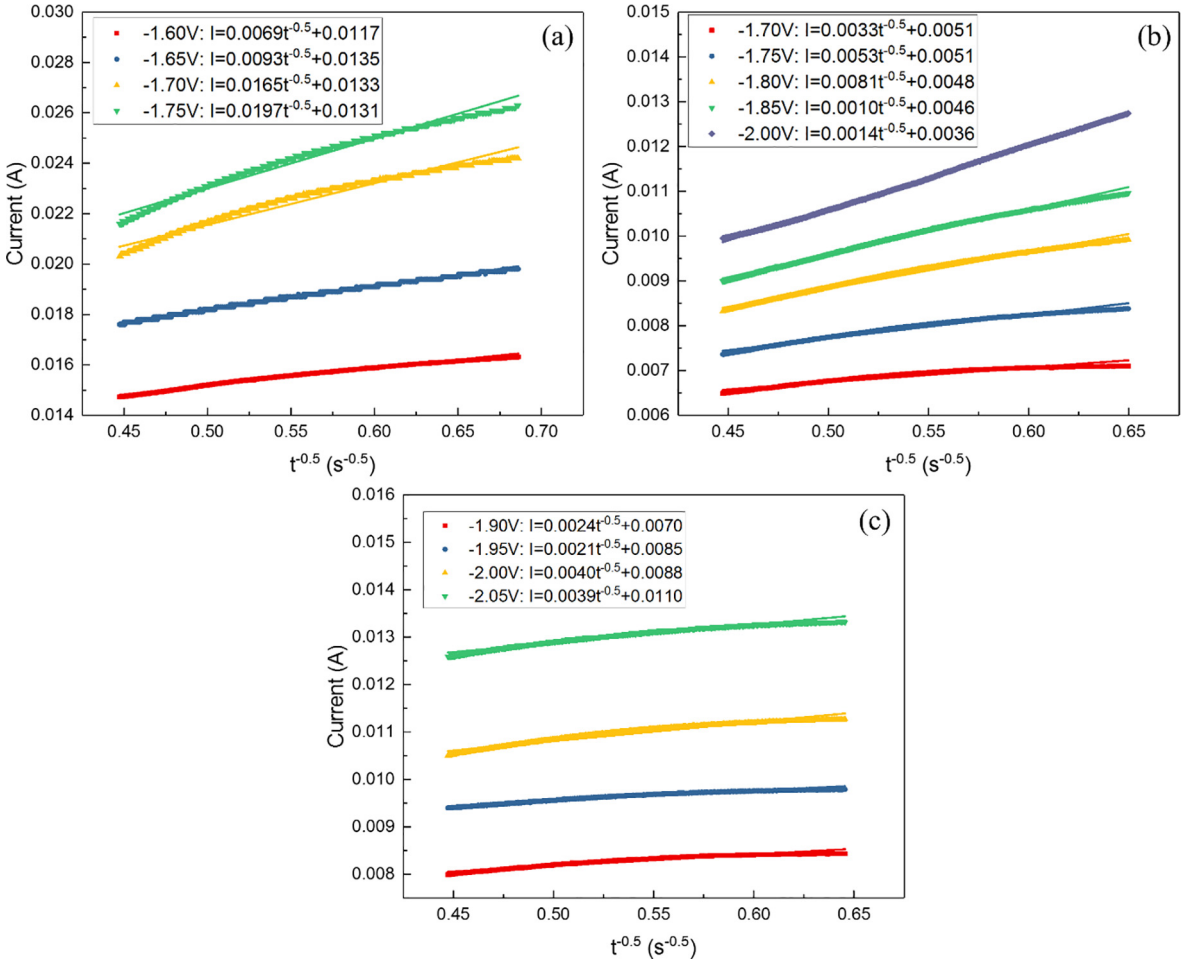

Fig. 7. Variation of current (I) with time ($t^{-0.5}$) at different applied potentials at 363 K for three ILs ((a) EMIC-$AlCl_3$, (b) BMIC-$AlCl_3$, and (c) HMIC-$AlCl_3$).

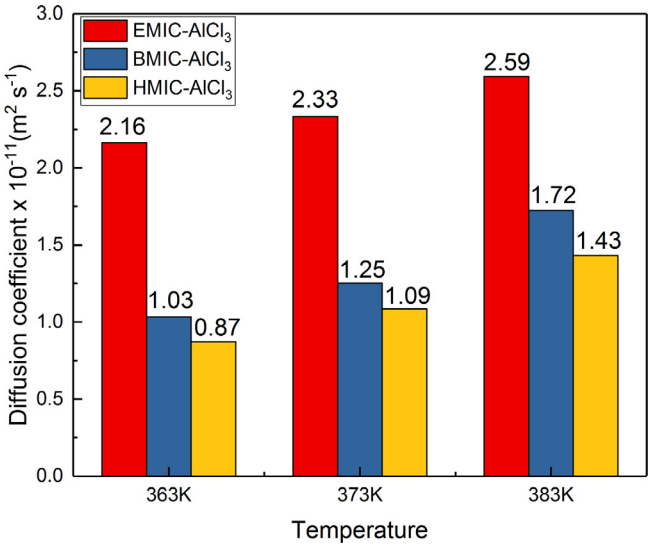

Fig. 8. Comparison of the diffusion coefficient of $Al_2Cl_7^-$ ions in different ionic liquids at various temperatures.

anion in the HMIC-$AlCl_3$ is the lowest, followed by BMIC-$AlCl_3$ and EMIC-$AlCl_3$.

Based on the Stokes-Einstein relation, a larger molecular size or viscosity of liquid causes a lowering the diffusion coefficient value according to equation (17) [37].

$$D \cdot \eta = \frac{k_B T}{c\pi\sigma_H} \tag{17}$$

where D is the diffusion coefficient ($m^2\ s^{-1}$), η is viscosity (Pa s), k_B is Boltzmann constant, T is the absolute temperature (K), c is numerical constant, and σ_H is the hydrodynamic diameter.

As it is known, HMIC has a larger molecular weight and hydrocarbon groups than EMIC or BMIC. Thus, the molecular size in HMIC-$AlCl_3$ IL is larger. In addition, HMIC-$AlCl_3$ has a relatively strong interaction force because of which the viscosity of HMIC-$AlCl_3$ is higher than the other two ILs [22,38]. These two reasons cause the diffusion coefficient of $Al_2Cl_7^-$ ion lower in the HMIC-$AlCl_3$ IL. In addition, it has been illustrated that the same cation with a smaller anion will result in higher diffusivity of cation and anion [39]. Therefore, the same anion with smaller cations will have a similar result.

The calculated diffusion coefficient of $Al_2Cl_7^-$ species in the present study is also compared with literature data, which are listed in Table 3. The little difference might due to the different concentrations of $Al_2Cl_7^-$ species in the ionic liquid or different types of the ionic liquid. And the result calculated in the present study is reasonable as it is calculated based on the cylindrical electrode instead of the planar electrode.

3.3.2. Number density of nucleation and grain size of nuclei

As the electrodeposition of Al in three ILs follows three-dimension instantaneous nucleation and diffusion-control process, the number density of nucleation at different overpotentials can be calculated based on the model developed by Gunawardena *et al.* [33][40]. The relation is given by equations (18) and (19).

Table 3
Comparison of the diffusion coefficient of $Al_2Cl_7^-$ in the ionic liquids with literature data.

Ionic liquids(molar ratios)	$[Al_2Cl_7^-]$(mol m^{-3})	T(K)	Method	D(m^2 s^{-1})	Reference
BupyCl–$AlCl_3$ (1:2)	1.17×10^3	370	CV (R&S Eqn.)	21.4×10^{-11}	[44]
BupyCl–$AlCl_3$ (1:2)	1.17×10^3	303	CV (R&S Eqn.)	4.70×10^{-11}	[44]
BMIC–$AlCl_3$ (1:1.5)	–	298	CV (R&S Eqn.)	1.13×10^{-11}	[22]
TMPAC–$AlCl_3$ (1:2)	–	298	CV (R&S Eqn.)	2.17×10^{-11}	[29]
EMIC–$AlCl_3$ (1:1.5)	1.8185×10^3	363	CA (S&H. Eqn.)	$5.20–6.89 \times 10^{-11}$	[6]
BMIC–$AlCl_3$ (1:1.5)	1.8185×10^3	363	CA (S&H. Eqn.)	2.20×10^{-11}	[6]
BMIC–$AlCl_3$ (1:1.5)	–	298	CA (S&H. Eqn.)	3.90×10^{-11}	[22]
EMIC–$AlCl_3$ (1:1.1)	–	348	CA (S&H. Eqn.)	6.80×10^{-11}	[45]
EMIC–$AlCl_3$ (1:1.5)	1.8185×10^3	363	CA (Cot. Eqn.)	1.30×10^{-11}	[6]
BMIC–$AlCl_3$ (1:1.5)	1.8185×10^3	363	CA (Cot. Eqn.)	1.50×10^{-11}	[6]
TMPAC–$AlCl_3$ (1:2)	–	298	CA (Cot. Eqn.)	$2.03–4.12 \times 10^{-11}$	[29]
EMIC–$AlCl_3$ (1:2)	2.58×10^3	363	CA (Rev. Eqn.)	2.16×10^{-11}	Present
BMIC–$AlCl_3$ (1:2)	2.32×10^3	363	CA (Rev. Eqn.)	1.03×10^{-11}	Present
HMIC–$AlCl_3$ (1:2)	2.09×10^3	363	CA (Rev. Eqn.)	0.87×10^{-11}	Present

Table 4
The calculated number of nucleation density (N) and the grain size (r) of the deposition of Al in three ILs using Pt reference electrode at 363 K.

Potential vs. Pt (V)	EMIC-$AlCl_3$ N $\times 10^{11}$(m^{-2})	r $\times 10^{-6}$ (m)	BMIC-$AlCl_3$ N $\times 10^{11}$(m^{-2})	r $\times 10^{-6}$ (m)	HMIC-$AlCl_3$ N $\times 10^{11}$(m^{-2})	r $\times 10^{-6}$ (m)
−1.60	0.64	2.22	–	–	–	–
−1.65	1.01	1.78	–	–	–	–
−1.70	1.52	1.45	0.92	1.86	–	–
−1.75	1.87	1.30	1.33	1.55	–	–
−1.80	–	–	1.99	1.27	–	–
−1.85	–	–	2.84	1.06	–	–
−1.90	–	–	3.74	0.92	0.88	1.90
−1.95	–	–	–	–	1.19	1.64
−2.00	–	–	–	–	1.59	1.42
−2.05	–	–	–	–	2.20	1.20

$$j_m = 0.6382nFCD(kN)^{0.5} \quad (18)$$

$$k = (8\pi CM/\rho)^{0.5} \quad (19)$$

where j_m is peak current density (A m^{-2}), n is the number of exchanged electrons (0.75), F is the Faraday constant (96485C mol^{-1}), C is the concentration of $Al_2Cl_7^-$ ions, D is the diffusion coefficient (m^2 s^{-1}), k is a numerical constant, M is the atomic weight of aluminum (26.98 g mol^{-1}), and ρ is the density of metallic aluminum (2700 kg m^{-3}). Thus the grain size can be calculated based on the number density of nucleation [41] using equation (20).

$$r = (1/\pi N)^{0.5} \quad (20)$$

where r is the average radius of the grains (m), and N is the number density of nucleation (m^{-2}). The grain shape is assumed to be spherical. The calculated number density of nucleation and grain size in three ILs at different overpotentials is listed in Table 4.

As shown in Table 4, as the applied overpotential increases, the average radius of grains decreases, while the number density increases. This trend is in good agreement with the nucleation of other elements in the ionic liquid, such as Zn and Pb [30,42]. In addition, the calculated number density of nucleation from this study is in good

Table 5
Comparison of calculated number density of Al and other elements in different ionic liquids.

Conditions	N $\times 10^{11}$(m^{-2})	Reference
Al in EMIC-$AlCl_3$ (2.0), −1.75 V vs. Pt on W (WE), 363 K	1.87	Present
Al in BMIC-$AlCl_3$ (2.0), −1.75 V vs. Pt on W (WE), 363 K	1.33	Present
Al in HMIC-$AlCl_3$ (2.0), −1.95 V vs. Pt on W (WE), 363 K	1.19	Present
Al in EMIC-$AlCl_3$ (1.5), −0.60 V vs. Al on Cu (WE), 363 K	9.00	[6]
Al in BMIC-$AlCl_3$ (1.5), −0.60 V vs. Al on Cu (WE), 363 K	1.50	[6]
Al in TMPAC-$AlCl_3$ (2.0), −0.15 V vs. Al on W (WE), 333 K	36.9	[4]
Al in TMPAC-$AlCl_3$ (2.0), −0.15 V vs. Al on Al (WE), 333 K	2.31	[4]
Al in EMIC-$AlCl_3$ (1.1), 0.15 vs. Al on W (WE), 333 K	1.47	[45]
Al in EMIC-$AlCl_3$ (1.1), 0.25 vs. Al on GC (WE), 348 K	0.42	[45]
Al in EMIC-$AlCl_3$ (1.1), 0.50 vs. Al on taC:N (WE), 348 K	0.37	[45]
Zn in Urea-BMIC, −1.30 V vs. Ag on W (WE), 373 K	0.41	[42]
Pb in Urea-BMIC, −0.35 V vs. Ag on Cu (WE), 373 K	1.03	[30]

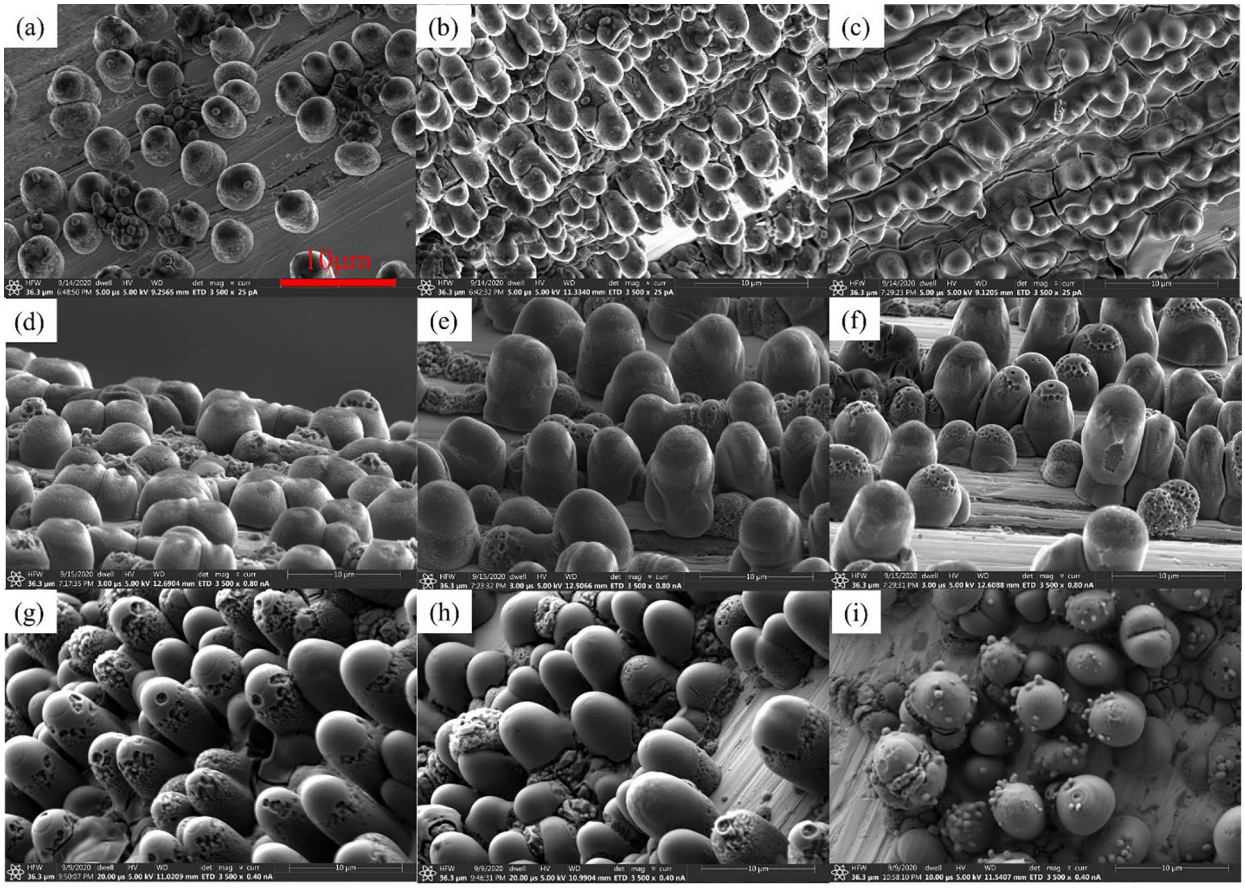

Fig. 9. SEM micrographs of Al deposit on W wire obtained in three ILs at 363 K with different potentials vs. Pt for 30 s ((a) −1.65 V in EMIC-$AlCl_3$, (b) −1.70 V in EMIC-$AlCl_3$, (c) −1.75 V in EMIC-$AlCl_3$, (d) −1.70 V in BMIC-$AlCl_3$, (e) −1.75 V in BMIC-$AlCl_3$, (f) −1.80 V in BMIC-$AlCl_3$, (g) −1.90 V in HMIC-$AlCl_3$, (h) −1.95 V in HMIC-$AlCl_3$, (i) −2.00 V in HMIC-$AlCl_3$).

agreement with the data reported in the literature, as shown in Table 5.

SEM micrographs indicate that the grain sizes are slightly decreased with at higher applied potential, which are comparable to the calculated result. The grain sizes for EMIC-$AlCl_3$ at three potentials are around 2-μm in diameter, which is in the same range as calculated. In addition, the grain sizes for BMIC-$AlCl_3$ and HMIC-$AlCl_3$ are in the range of 3–6 μm and 2–4 μm, respectively. These are comparable to the calculated grain values at a given potential. The reason for the little difference might be the heterogeneous nucleation during the electrodeposition process. In the literature [6], the grain sizes obtained from SEM are in the range of 0.5–2 μm at 363 K for EMIC-$AlCl_3$ system after 15 s electrodeposition. Moreover, the grain size of Al after deposition at −0.2 V vs. Al for TMPAC-$AlCl_3$ at 333 K is around 10 μm f]. This suggest that the grain sizes of nucleation estimated experimentally are in good agreement with the literature data. Besides, the shape of nucleation is spherical but grows oval, especially at more negative potentials. One reason might be that there is no space for them to grow in the horizontal direction. Another reason could be the concentration gradient and surface energy. The first nucleation on the substrate will form a peak part, which has a steeper concentration gradient than in the electrolyte near the flat part [43]. To minimize the surface energy at the peak part, the further deposit prefers to nucleate at the peak parts, as shown in Fig. 9(i). Thus, the peak parts grow more and more, thereby resulting in an oval shaped-morphology. However, when surface diffusion of deposits is not significant, the further nuclei will grow in other directions forming the dendrites [43]. As shown in Fig. 9(b), (e), and (f), several grains are growing on top of initial oval-shaped grain. If the growth time is sufficiently high, then the vertical growth of grains may turn into other directions forming dendrites. An interesting point in the mechanism of grain growth is that internal stress increases as the grains merge into each other. And the internal stress may cause the formation of crevices on the deposited material, as shown in Fig. 9(c).

3.4. Structural analysis of Al deposits

The surface morphology and elemental composition of the Al electrodeposit obtained from EMIC-$AlCl_3$, BMIC-$AlCl_3$ and HMIC-$AlCl_3$ electrolytes at − 1.7 V (vs. Pt) at 363 K on a Cu substrate is shown in Fig. 10. The SEM micrograph indicates dendrite formation on the Cu substrate, which is significantly higher for the EMIC-$AlCl_3$ ionic liquid. Higher dendrites formation might be due to the higher overpotential during the electrodeposition process. In addition, the peaks in the EDS spectrum are mainly attributed to electrodeposited Al and the Cu substrate. No oxygen peak was detected, indicating that the deposition obtained is of pure metallic Al. The XRD analysis of the Al deposits are also performed. For this purpose, the deposits were scratched from the sample obtained using EMIC-$AlCl_3$ and is shown in Fig. 11. The peaks in the XRD data match well with that of standard Al diffraction pattern (ICDD #01–071-3760). No impurity peaks or phases are detected from XRD as well as SEM-EDS analysis.

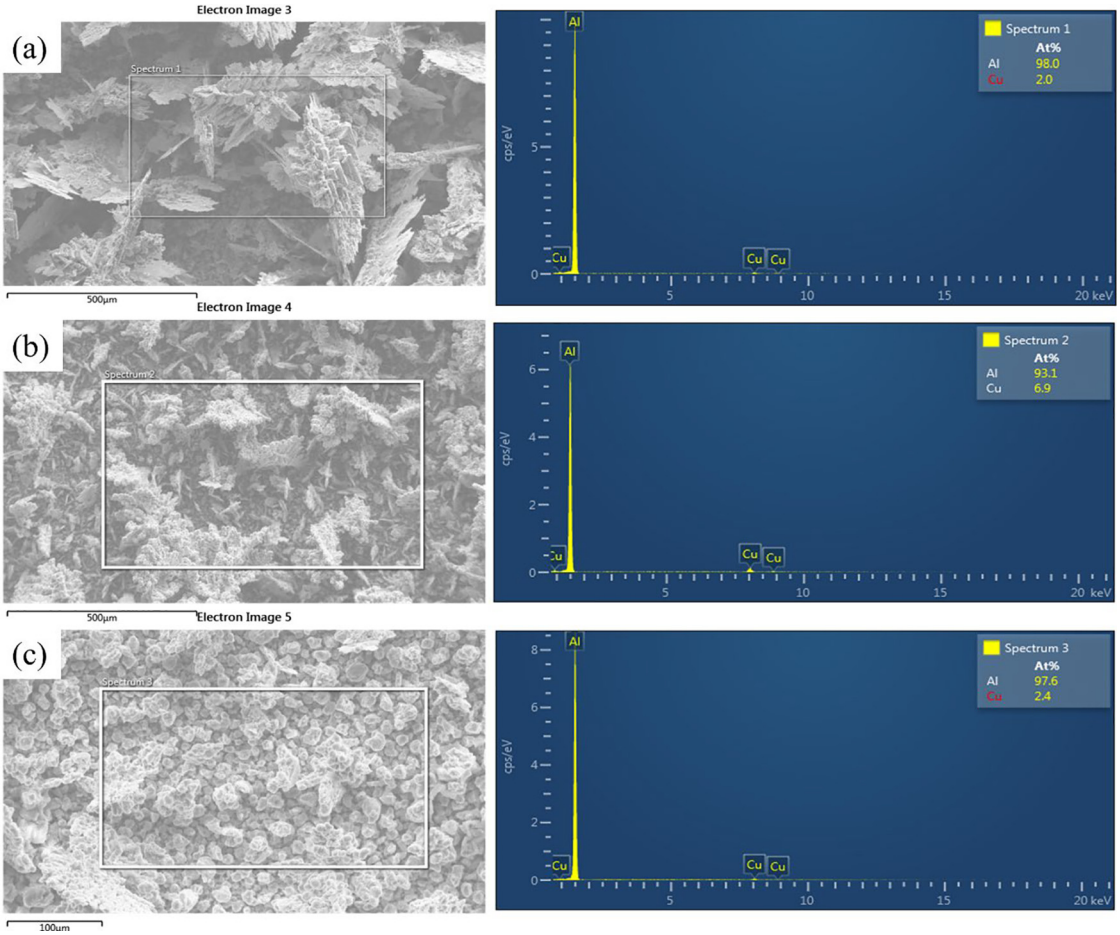

Fig. 10. The SEM images and corresponding EDS of Al deposited obtained on Cu substrate for 1 h at −1.7 V vs. Pt from three ionic liquid ((a) EMIC-$AlCl_3$ (b) BMIC-$AlCl_3$ and (c) HMIC-$AlCl_3$).

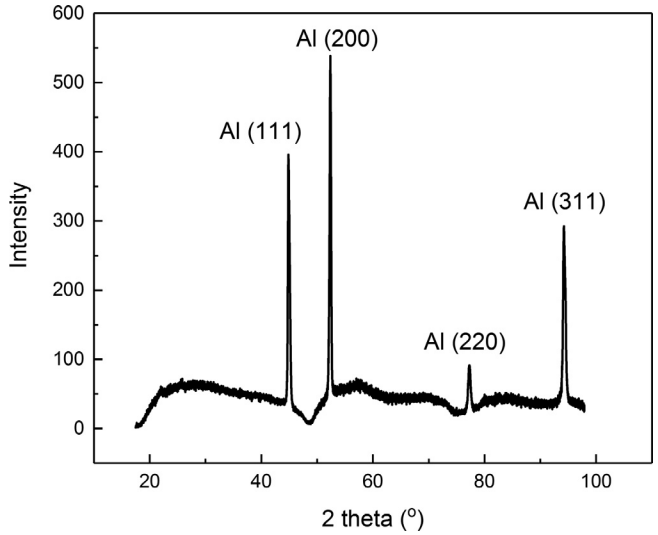

Fig. 11. Representative XRD of Al deposit (Al deposited obtained on Cu substrate for 1 h at −1.7 V vs. Pt from EMIC-$AlCl_3$).

4. Conclusions

The electrochemical behaviors of $Al_2Cl_7^-$ species in EMIC-$AlCl_3$, BMIC-$AlCl_3$, and HMIC-$AlCl_3$ (1:2) ionic liquids were investigated at different temperatures (363 to 383 K). The cyclic voltammograms illustrated that reduction of $Al_2Cl_7^-$ to metallic Al was a quasi-reversible process. The cathodic peak current density in EMIC-$AlCl_3$ was higher, and the applied potential was less negative. The chronoamperometric analysis indicated that the nucleation of Al on the tungsten working electrode was an instantaneous nucleation process. The diffusion coefficients of $Al_2Cl_7^-$ species were calculated in three ionic liquids at different temperatures using different methods. However, the Scharifker and Hills equation and the Cottrell equation are used for the planar diffusion process. For the cylindrical electrode, the diffusion coefficient values calculated using the revised method at 363 K are 2.16×10^{-11}, 1.03×10^{-11}, and 0.87×10^{-11} $m^2\ s^{-1}$ for EMIC-$AlCl_3$, BMIC-$AlCl_3$, and HMIC-$AlCl_3$, respectively, which are comparable to the literature data. The diffusion coefficient was the largest in EMIC-$AlCl_3$ and followed by BMIC-$AlCl_3$ and then HMIC-$AlCl_3$. The reasons are 1) the viscosity of HMIC-$AlCl_3$ is the largest, and 2) the molecular size of the cation in HMIC-$AlCl_3$ is the largest. The current work presents significant progress in the study of the diffusion coefficient of $Al_2Cl_7^-$ species in such ILs that includes 1) calculation of the concentration of $Al_2Cl_7^-$ species based on thermodynamic data; 2) use and comparison of different methods to precisely determine the diffusion coefficient values; especially for the cylindrical electrode, 3) establishing the relationship between several factors and the diffusion coefficient (the diffusion coefficient of $Al_2Cl_7^-$ increased with temperature, while decreased as hydrocarbon group or viscosity of the IL is increased). Besides, the calculated number density of nucleation is comparable to the literature result. And the calculated grain sizes in the present work are not only in good agreement with the experimen-

tal result but also in a similar range as the literature data. The little difference might due to the heterogeneous nucleation in the deposition process. The oval-shaped grains of deposits are detected in three ILs, and the mechanism of the grain growth is simply discussed in the present work. The SEM-EDS and XRD analyses suggested that electrodeposits consisted of pure metallic Al phase without any impurities or oxygen.

CRediT authorship contribution statement

Yuxiang Peng: Methodology, Formal analysis, Writing - original draft. **Pravin S. Shinde:** Formal analysis, Writing - review & editing. **Ramana G. Reddy:** Formal analysis, Writing - review & editing, Conceptualization.

Declaration of Competing Interest

The authors declare that they have no known competing financial interests or personal relationships that could have appeared to influence the work reported in this paper.

Acknowledgments

The authors acknowledge the financial support received from the National Science Foundation (CMMI-MEP 1762522), the Department of Energy (DOE), and the ACIPCO for this research project. We also thank the Department of Metallurgical and Materials Engineering (MTE) and the University of Alabama for providing experimental and analytical facilities.

References

[1] W. Barabasz, D. Albinska, M. Jaskowska, J. Lipiec, Ecotoxicology of aluminium, Pol. J. Environ. Stud. 11 (3) (2002) 199–204.
[2] W. Haupin, Electrochemistry of the Hall-Heroult process for aluminum smelting, J. Chem. Educ. 60 (4) (1983) 279–282.
[3] D. Pradhan, R.G. Reddy, Dendrite-free aluminum electrodeposition from $AlCl_3$–1-ethyl-3-methyl-imidazolium chloride ionic liquid electrolytes, Metall. Mater. Tran. B 43 (3) (2012) 519–531.
[4] T. Jiang, M.C. Brym, G. Dubé, A. Lasia, G. Brisard, Electrodeposition of aluminium from ionic liquids: Part II-studies on the electrodeposition of aluminum from aluminum chloride ($AlCl_3$)-trimethylphenylammonium chloride (TMPAC) ionic liquids, Surf. Coat. Technol. 201 (1–2) (2006) 10–18.
[5] J.-K. Chang, S.-Y. Chen, W.-T. Tsai, M.-J. Deng, I.-W. Sun, Electrodeposition of aluminum on magnesium alloy in aluminum chloride ($AlCl_3$) –1-ethyl-3-methylimidazolium chloride (EMIC) ionic liquid and its corrosion behavior, Electrochem. Commun. 9 (7) (2007) 1602–1606.
[6] D. Pradhan, R.G. Reddy, Mechanistic study of Al electrodeposition from EMIC–$AlCl_3$ and BMIC–$AlCl_3$ electrolytes at low temperature, Mater. Chem. Phys. 143 (2) (2014) 564–569.
[7] R.G. Reddy, Ionic liquids: How well do we know them?, J. Phase Equilib. Diff. 27 (3) (2006) 210–211.
[8] H. Yang, R.G. Reddy, Electrochemical kinetics of reduction of zinc oxide to zinc using 2: 1 urea/ChCl ionic liquid, Electrochim. Acta 178 (2015) 617–623.
[9] H. Ohno, Electrochemical aspects of ionic liquids, John Wiley & Sons, New Jersey, 2005.
[10] R.T. Carlin, P.C. Trulove, H.C. De Long, Electrodeposition of Cobalt-Aluminum alloys from room temperature chloroaluminate molten salt, J. Electrochem. Soc. 143 (9) (1996) 2747–2758.
[11] J. Robinson, R. Osteryoung, The electrochemical behavior of aluminum in the low temperature molten salt system n butyl pyridinium chloride: aluminum chloride and mixtures of this molten salt with benzene, J. Electrochem. Soc. 127 (1) (1980) 122–128.
[12] P.K. Lai, M. Skyllas-Kazacos, Electrodeposition of aluminium in aluminium chloride/1-methyl-3-ethylimidazolium chloride, J. Electroanal. Chem. Interf. Electrochem. 248 (2) (1988) 431–440.
[13] D. Pradhan, R.G. Reddy, Electrochemical production of Ti–Al alloys using $TiCl_4$–$AlCl_3$–1-butyl-3-methyl imidazolium chloride (BMIMCl) electrolytes, Electrochim. Acta 54 (6) (2009) 1874–1880.
[14] P. Koronaios, D. King, R.A. Osteryoung, Acidity of neutral buffered 1-ethyl-3-methylimidazolium chloride – $AlCl_3$ ambient-temperature molten salts, Inorg. Chem. 37 (8) (1998) 2028–2032.
[15] V. Kamavaram, D. Mantha, R. Reddy, Recycling of aluminum metal matrix composite using ionic liquids: Effect of process variables on current efficiency and deposit characteristics, Electrochim. Acta 50 (16–17) (2005) 3286–3295.
[16] V. Kamavaram, D. Mantha, R.G. Reddy, Electrorefining of aluminum alloy in ionic liquids at low temperatures, J. Min. Metall. B 39 (1-2) (2003) 43–58.
[17] Y. Zheng, C. Peng, Y. Zheng, D. Tian, Y. Zuo, Y. Zheng, Low-temperature electrolysis of aluminium from 1-butyl-3-methylimidazolium chloroaluminate ionic liquids with inert anode, Int. J. Electrochem. Sci. 11 (2016) 6095–6109.
[18] T. Jiang, M.C. Brym, G. Dubé, A. Lasia, G. Brisard, Electrodeposition of aluminium from ionic liquids: Part I—electrodeposition and surface morphology of aluminium from aluminium chloride ($AlCl_3$)–1-ethyl-3-methylimidazolium chloride ([EMIM]Cl) ionic liquids, Surf. Coat. Technol. 201 (1–2) (2006) 1–9.
[19] H. Lang, J. Zhang, Y. Kang, S. Chen, S. Zhang, Effects of lithium bis (oxalato) borate on electrochemical stability of [Emim][Al_2Cl_7] ionic liquid for aluminum electrolysis, Ionics 23 (4) (2017) 959–966.
[20] J. Lu, D. Dreisinger, Electrochemistry: Ionic Liquid Electroprocessing of Reactive Metals, Ionic Liquid as Green Solvents 39 (2003) 495–508.
[21] J. Tang, K. Azumi, Optimization of pulsed electrodeposition of aluminum from $AlCl_3$-1-ethyl-3-methylimidazolium chloride ionic liquid, Electrochim. Acta 56 (3) (2011) 1130–1137.
[22] V. Kamavaram, Novel electrochemical refining of aluminum based materials in low temperature ionic liquid electrolytes, The University of Alabama, 2004.
[23] Z.J. Karpinski, R.A. Osteryoung, Determination of equilibrium constants for the tetrachloroaluminate ion dissociation in ambient-temperature ionic liquids, Inorg. Chem. 23 (10) (1984) 1491–1494.
[24] G. Zhu, M. Angell, C.-J. Pan, M.-C. Lin, H. Chen, C.-J. Huang, J. Lin, A.J. Achazi, P. Kaghazchi, B.-J. Hwang, Rechargeable aluminum batteries: effects of cations in ionic liquid electrolytes, RSC advances 9 (20) (2019) 11322–11330.
[25] B. Li, C. Fan, Y. Chen, J. Lou, L. Yan, Pulse current electrodeposition of Al from an AlCl3-EMIC ionic liquid, Electrochim. Acta 56 (16) (2011) 5478–5482.
[26] B.K.K. Kasem, S. Jones, Platinum as a reference electrode in electrochemical measurements, Platinum Met. Rev. 52 (2) (2008) 100–106.
[27] X. Wen, Y. Liu, D.a. Xu, Y. Zhao, R.K. Lake, J. Guo, Room-Temperature Electrodeposition of Aluminum via Manipulating Coordination Structure in $AlCl_3$ Solutions, The journal of physical chemistry letters 11 (4) (2020) 1589–1593.
[28] A.J. Bard, L.R. Faulkner, J. Leddy, C.G. Zoski, Electrochemical methods: fundamentals and applications, Wiley, New York, 1980.
[29] Y. Zhao, T.J. VanderNoot, Electrodeposition of aluminium from room temperature $AlCl_3$-TMPAC molten salts, Electrochim. Acta 42 (11) (1997) 1639–1643.
[30] A. Liu, Z. Shi, R.G. Reddy, Electrodeposition of Pb from PbO in urea and 1-butyl-3-methylimidazolium chloride deep eutectic solutions, Electrochim. Acta 251 (10) (2017) 176–186.
[31] H. Yang, R.G. Reddy, Electrochemical deposition of zinc from zinc oxide in 2: 1 urea/choline chloride ionic liquid, Electrochim. Acta 147 (20) (2014) 513–519.
[32] B. Scharifker, G. Hills, Theoretical and experimental studies of multiple nucleation, Electrochim. Acta 28 (7) (1983) 879–889.
[33] G. Gunawardena, G. Hills, I. Montenegro, B. Scharifker, Electrochemical nucleation: part I. general considerations, J. Electroanal. Chem. Interf, Electrochem. 138 (2) (1982) 225–239.
[34] H. Yang, R.G. Reddy, Fundamental studies on electrochemical deposition of lead from lead oxide in 2: 1 urea/choline chloride ionic liquids, J. Electrochem. Soc. 161 (10) (2014) D586–D592.
[35] X.-H. Xu, C.L. Hussey, Electrodeposition of Silver on Metallic and Nonmetallic Electrodes from the Acidic Aluminum Chloride-1-Methyl-3-Ethylimidazolium Chloride Molten Salt, J. Electrochem. Soc. 139 (5) (1992) 1295–1300.
[36] Y.-M. Fang, J.-J. Sun, G.-N. Chen, A Simple Approach to the Solution of the Diffusion Equation at the Microcylinder Electrode—an Inspiration from the Film Projector, ChemPhysChem 10 (14) (2009) 2393–2396.
[37] L. Costigliola, D.M. Heyes, T.B. Schrøder, J.C. Dyre, Revisiting the Stokes-Einstein relation without a hydrodynamic diameter, J. Chem. Phys. 150 (2) (2019) 021101, https://doi.org/10.1063/1.5080662.
[38] Y. Zheng, K. Dong, Q. Wang, J. Zhang, X. Lu, Density, viscosity, and conductivity of Lewis acidic 1-butyl-and 1-hydrogen-3-methylimidazolium chloroaluminate ionic liquids, J. Chem. Eng. Data 58 (1) (2013) 32–42.
[39] F. Makhlooghiazad, J. Guazzagaloppa, L.A. O'Dell, R. Yunis, A. Basile, P.C. Howlett, M. Forsyth, The influence of the size and symmetry of cations and anions on the physicochemical behavior of organic ionic plastic crystal electrolytes mixed with sodium salts, Phys. Chem. Phys. Chem. 20 (7) (2018) 4721–4731.
[40] G.A. Gunawardena, G.J. Hills, I. Montenegro, Potentiostatic studies of electrochemical nucleation, Electrochim. Acta 23 (8) (1978) 693–697.
[41] R.T. Carlin, W. Crawford, M. Bersch, Nucleation and morphology studies of aluminum deposited from an ambient-temperature chloroaluminate molten salt, J. Electrochem. Soc. 139 (10) (1992) 2720–2727.
[42] A. Liu, Z. Shi, R.G. Reddy, Electrodeposition of zinc from zinc oxide in 2: 1 urea/1-butyl-3-methylimidazolium chloride ionic liquid, J. Electrochem. Soc. 164 (9) (2017) D666–D673.
[43] K. Fukami, S. Nakanishi, H. Yamasaki, T. Tada, K. Sonoda, N. Kamikawa, N. Tsuji, H. Sakaguchi, Y. Nakato, General mechanism for the synchronization of electrochemical oscillations and self-organized dendrite electrodeposition of metals with ordered 2D and 3D microstructures, J. Chem. Phys. C 111 (3) (2007) 1150–1160.
[44] J. Robinson, R.A. Osteryoung, An electrochemical and spectroscopic study of some aromatic hydrocarbons in the room temperature molten salt system aluminum chloride-n-butylpyridinium chloride, J. Am. Chem. Soc. 101 (2) (1979) 323–327.
[45] J.-J. Lee, B. Miller, X.u. Shi, R. Kalish, K.A. Wheeler, Aluminum deposition and nucleation on nitrogen-incorporated tetrahedral amorphous carbon electrodes in ambient temperature chloroaluminate melts, J. Electrochem. Soc. 147 (9) (2000) 3370, https://doi.org/10.1149/1.1393908.